Published in "Soft Matter 6(18): 4536-4539 , 2010"
which should be cited to refer to this work.

Surface-specific ordering of reverse micelles in confinement

Kim Nygård,*[a] Dillip K. Satapathy,[b] Edith Perret,[c] Celestino Padeste,[c] Oliver Bunk,[c] Christian David[c] and J. Friso van der Veen[de]

We have applied holographic X-ray diffraction from fluid-filled channel arrays for model-independent density reconstruction of spherical AOT/water/isooctane reverse micelles (average diameter $\sigma \simeq 12$–13 nm) confined between planar surfaces. We find the confinement-induced ordering of the reverse micelles to strongly depend on the surface potential of the confining surfaces: for hydrophilic surfaces we find diffuse monolayers centered at 13 ± 3 nm away from the solid–fluid interface, while for hydrophobic surfaces we observe close-packed monolayers at the solid–fluid interface.

1 Introduction

Confined complex fluids are abundant in nature, such as blood in capillary vessels and proteins in narrow pores. In terms of possible applications, the examples range from micelle-based drug delivery to food technology. The confinement is known to induce ordering of the fluid along the confining direction, which in turn affects other properties such as the diffusion of the fluid constituents.[1] Consequently, a deep understanding of confinement-induced ordering of complex fluids is crucial. However, theoretical work is challenging, since the behavior of complex fluids in confinement is governed not only by excluded volume,[2] but also by more subtle interactions, such as electrostatic and hydrophobic forces, and a large disparity in size and charge between macroions and solvated ions. Hence, experimental studies are needed to guide theoretical work.

Traditionally confinement-induced ordering of complex fluids has been studied by surface-force experiments,[3] although such experiments do not directly reveal the density profile of the confined fluid.[4] Alternative approaches are provided by reflectivity[5] or small-angle scattering[6,7] using X-rays or neutrons, which can yield the fluid's structure with sub-nanometer resolution. However, since the phase information is (generally) lost in such experiments, the real-space structure has to be determined by modeling the reciprocal-space reflectivity or scattering curve, and is therefore not unambiguous; this is demonstrated, for example, by the conflicting interpretations either in favor of or against a vaporlike depletion region - the so-called hydrophobic gap - between water and hydrophobic surfaces.[8,9]

Here we apply a different approach to address the ordering of reverse micelles of AOT [also known as sodium bis(2-ethylhexyl) sulfosuccinate], water, and isooctane confined between planar surfaces, which is based on X-ray diffraction (XRD) from fluid-filled channel arrays combined with phase-retrieval methods. For phase retrieval we use a recently developed grating-based holographic XRD technique,[10,11] which allows us to reconstruct the confined fluid's density profile in a model-independent manner by direct Fourier inversion. In contrast to surface-force experiments, we apply no external force on the confined fluid within this approach. We obtain unambiguous experimental evidence for surface-specific ordering of confined reverse micelles: for hydrophilic confining surfaces, we observe ordering into diffuse layers of reverse micelles centered at 13 ± 3 nm away from the solid–fluid interfaces, while for hydrophobic confining surfaces, we observe monolayers of close-packed reverse micelles at the solid–fluid interfaces. In both cases, we observe no ordering beyond a monolayer close to the solid–fluid interface, an effect which we primarily attribute to a large polydispersity of the reverse micelles.

2 Experimental

The sample consisted of spherical AOT/water/isooctane reverse micelles (Fig. 1) in the so-called water-in-oil microemulsion or L_2 phase,[12] *i.e.*, spherical water droplets (Milli-Q) covered by a monolayer of AOT ($C_{20}H_{37}NaO_7S$, Sigma-Aldrich, purity ≥ 99%) dispersed in isooctane (Fluka, purity ≥ 99.5%). At the temperature and low water concentrations of the present study, the surfactant AOT forms spherical reverse micelles, with the droplet size depending on the molar ratio $w_0 = [H_2O]/[AOT]$ of water and AOT. We used two different reverse micelles with molar ratios $w_0 = 48$ (henceforth denoted #1) and $w_0 = 37$ (denoted #2) [see below for the small-angle X-ray scattering (SAXS) characterization of the bulk reverse micelles].

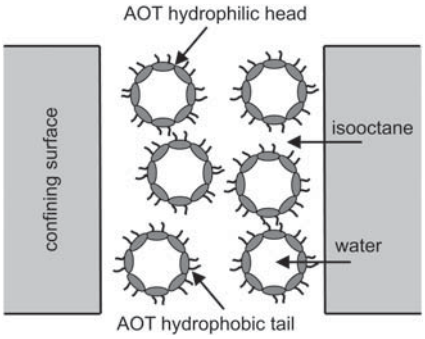

Fig. 1 Schematic of AOT/water/isooctane reverse micelles confined between hydrophilic or hydrophobic planar surfaces (not drawn to scale).

[a]*Paul Scherrer Institut, CH-5232 Villigen PSI, Switzerland. E-mail: kim.nygard@psi.ch*
[b]*University of Fribourg, CH-1700 Fribourg, Switzerland*
[c]*Paul Scherrer Institut, CH-5232 Villigen PSI, Switzerland*
[d]*Paul Scherrer Institut, CH-5232 Villigen PSI, Switzerland*
[e]*ETH Zürich, CH-8093 Zürich, Switzerland*

For confinement we used silicon channel arrays, *i.e.*, linear diffraction gratings, with the following parameters: a period of $p = 400$ nm, channel width in the range $w \simeq 120$–170 nm, and a depth of $h \simeq 2$ μm. The confining surfaces are structureless on the length scale of the AOT/water droplets, which is a prerequisite for observing confinement-induced fluid ordering. Moreover, the channel arrays serve as momentum-transfer calibration standards for the SAXS characterization.[13] The reader is referred to ref. 11 for details about the fabrication of the channel arrays. In order to study the effect of the surface potential, we used channel arrays with two different surface terminations: (i) one set of channel arrays was used without further preparation. Since these channel arrays were covered by a natural oxide layer, they had a hydrophilic termination (contact angle of water $\vartheta \simeq 60°$). (ii) Another set of channel arrays was coated by fluorinated silanes,[14] leading to a hydrophobic termination ($\vartheta \simeq 95°$).

We carried out the experiment at the cSAXS beamline (X12SA) of the Swiss Light Source, Paul Scherrer Institut. A schematic of the experimental setup is shown in Fig. 2. The incident X-rays impinged perpendicular to the channel array and we detected the scattered X-rays in transmission geometry 7 m behind the sample using the Pilatus 2M pixel detector.[15] The incident X-ray beam had a wavelength of $\lambda = 0.10$ nm and a beam size of 0.2×0.1 mm^2 (horizontal $\times$ vertical) at the sample position, and it was focused onto the detector plane in order to maximize the angular resolution. We placed an evacuated flight tube between the sample and the detector, in order to minimize parasitic scattering. We ruled out radiation-damage effects by collecting the diffraction data in sets of 10×1 and 10×10 s exposures and verifying that the individual diffraction patterns were consistent within the statistical accuracy. With this setup and channel arrays, we could reliably determine the diffraction efficiencies up to $M = 50$ diffraction orders, allowing a reconstruction of the density profile with a real-space sampling interval of $\Delta x = p/(2M + 1) \simeq 4.0$ nm. We carried out the experiment at room temperature, $T = 297$ K.

For characterization of the reverse micelles, we carried out SAXS experiments on the bulk fluids. Following ref. 16, we modeled the particle form factor using polydisperse, spherical water droplets (electron density $\rho_w = 334$ nm^{-3}) surrounded by a monolayer of polar AOT headgroups ($\rho_h \approx 850$ nm^{-3}) of thickness $d_h = 0.2$ nm. Since the AOT hydrocarbon tails have a density ρ_t close to that of isooctane ($\rho_i = 241$ nm^{-3}), they do not contribute to the form factor. We accounted for the polydispersity of the water droplets using the normalised Schulz distribution within the local monodisperse approximation.[17] We included the interparticle interactions using a sticky hard-sphere model,[18] which accounts for the surface adhesion of the particles. However, the data are well described by a fixed stickiness parameter $\tau = 100$, implying hard-sphere-like interparticle interactions. In determining the structure factor, we also included the length of the hydrocarbon tail, $d_t = 0.4$ nm, which increases both the particle size and the volume fraction. With this simple model, we can reasonably reproduce the SAXS data (see Fig. 3). We have verified that the contributions of cylindrical and dry spherical reverse micelles are negligible. Table 1 summarises the parameters of the modeling.

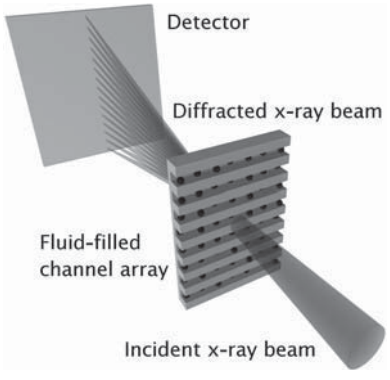

Fig. 2 Schematic of the experimental setup.

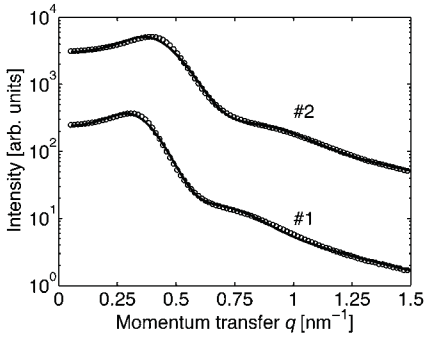

Fig. 3 SAXS characterization of the bulk AOT/water/isooctane reverse micelles (vertically offset for clarity). The circles denote the experimental data (only every tenth data point shown for clarity), while the solid lines depict a model of polydisperse spherical shells with sticky hard-sphere interparticle interactions (see text for details and Table 1 for the parameters of the model).

Table 1 Best-fit parameters for the bulk SAXS data: volume fraction ϕ of the spherical AOT/water droplets as well as average radius R and polydispersity $\Delta R/R$ of the water droplets (see text for details about the modeling)

#	ϕ	R [nm]	$\Delta R/R$
1	0.32	6.2	0.21
2	0.35	5.0	0.21

The ensemble-averaged electron density modulation $\Delta\rho(x) \equiv \rho(x) - \bar{\rho}$, with $\rho(x)$ denoting the electron density profile across the confining channel and $\bar{\rho}$ its average, can be quantitatively reconstructed from the XRD data in a model-independent manner using the grating-based holographic XRD technique:[10,11]

$$\Delta\rho(x) \simeq (\lambda h r_e)^{-1} \sum_{m=-M}^{M} \frac{(\eta_m - \eta_m^0)}{2\Phi\Re[F_m]} \cos(2\pi m x/p) \qquad (1)$$

Here η_m and $\eta_m{}^0$ denote the diffraction efficiencies for diffraction order m of the fluid-filled channel array and a reference array, respectively, F_m the theoretical form factor of the known channel array, Φ the average phase shift of the exit wave field across the solid–fluid interface, r_e the classical electron radius, and $\Re$ the real part of a complex quantity. It should be noted that the present XRD study of confined reverse micelles is more challenging, compared to our previous experiments on confined

colloids,[19,20] due to the following reasons: (i) The average particle diameter is smaller by a factor of ten ($\sigma \simeq$ 12–13nm for the reverse micelles compared to $\sigma \simeq 120$ nm for the colloidal particles). (ii) The contrast in the refractive index (for the used wavelengths) between water and isooctane ($\Delta\delta \simeq 0.43 \times 10^{-6}$) is a factor of three smaller than between silica and a solution of 55% benzyl alcohol and 45% ethanol ($\Delta\delta \simeq 1.37 \times 10^{-6}$). (iii) The polydispersity of the water droplets ($\Delta R/R \simeq 0.2$) is a factor of five larger than for the colloids ($\Delta R/R < 0.04$).

3 Results and discussion

First, we consider the ordering of reverse micelles between hydrophilic confining surfaces. The reconstructed $\Delta\rho(x)$ presented in Fig. 4 illustrates the ordering for selected channel widths. The most prominent features are a depletion of electron density close to the solid surface and a peak in the electron-density profile at a distance of 13 ± 3 nm from the solid–fluid interface. Within the accuracy of the present experiment, we observe no effect of the confining channel width on the above findings. We note that AOT/water/heptane reverse micelles confined between strongly hydrophilic mica surfaces in a surface-force apparatus have previously been found to exhibit a depletion region of several nanometers, which was attributed to the forming of layers of water and AOT at the mica surfaces.[21] However, considering the electron densities of isooctane, water, and AOT ($\rho_i < \rho_w < \rho_{AOT}$), the present observation necessarily implies an excess of isooctane rather than water and AOT at the hydrophilic surface. We therefore interpret the data of Fig. 4 as an ordering of the reverse micelles into diffuse monolayers centered at 13 ± 3 nm away from the confining surfaces. This, in turn, suggests a soft repulsive term in the effective particle-wall interaction potential, as previously observed in computational work on model oil/water/surfactant systems.[22]

For comparison, we also study the ordering of reverse micelles confined between hydrophobic surfaces (shown in Fig. 5). Most notably, we observe a large electron density excess at the solid–fluid interface. We emphasize that this observation does not conform with the archetypical system of a hard-sphere fluid at a hard surface,[23] which has previously been used, *e.g.*, to successfully model neutron reflectivity data from triblock copolymer micelles at hydrophilic surfaces.[24] Rather, the density excess indicates an attractive particle-wall interaction.[25] Integration of the density excess peak gives an areal electron density excess of $\Delta\rho_{2D} \simeq 230 \pm 40$ nm^{-2}, implying a local volume fraction $\phi_{2D} \simeq 0.56 \pm 0.04$ of spherical AOT/water droplets at the solid–fluid interface. This value is significantly larger than $\phi = 0.35$ obtained from the bulk. For comparison, the corresponding values assuming close-packed monolayers of hexagonal and square symmetry and the average particle diameter $\sigma \equiv 2(R + d_h + d_t)$ are $\phi_\Delta = 0.60$ and $\phi_\square = 0.52$, respectively. The good agreement between the latter values and the experimental result implies an ordering of the reverse micelles into close-packed monolayers at the solid–fluid interfaces. We expect the ordering into close-packed monolayers to strongly affect, for example, the diffusive properties of the confined fluid.[1]

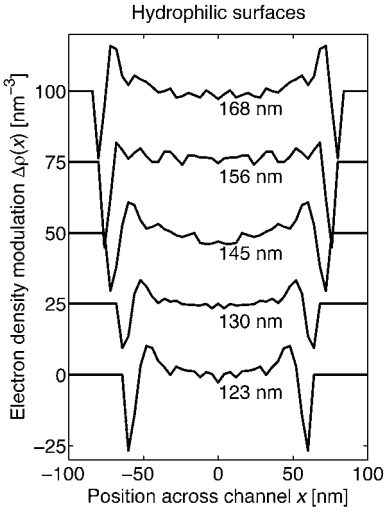

Fig. 4 Electron density modulation $\Delta\rho(x)$ of spherical AOT/water/isooctane reverse micelles #1 confined between hydrophilic planar surfaces. The density modulations for different channel widths are vertically offset by 25 nm^{-3} for clarity. The channel widths are given next to the density modulations.

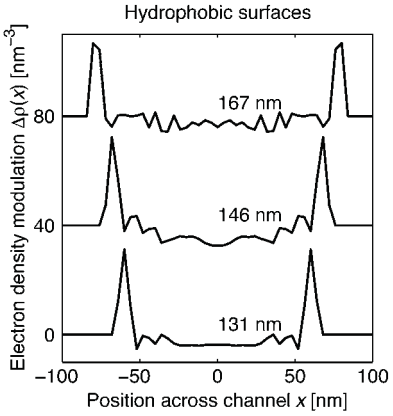

Fig. 5 As 4, except for hydrophobic confining surfaces and reverse micelle #2. The density modulations are vertically offset by 40 nm^{-3} for clarity.

The reconstructed electron density modulations presented here for hydrophilic *versus* hydrophobic confining surfaces exhibit systematic differences close to the solid–fluid interface. This observation, which we have verified for two sets of both hydrophilic and hydrophobic channel arrays, provides indisputable experimental evidence for surface-specific ordering of reverse micelles in confinement. Moreover, we note that these findings are irrespective of the confining channel width, implying that the confining surfaces act independently of each other in inducing the ordering.

Within the accuracy of the present study, we observe no confinement-induced fluid ordering beyond a monolayer close to the solid–fluid interface. This observation, which we predominantly attribute to a large polydispersity of the reverse micelles, can be rationalised as follows. For large confining channel widths, for which the fluid's density in the centre of the channel approaches the bulk value ρ_0, the asymptotic decay of the density profile $\rho(x)$ is given by[26,27]

$$\rho(x) - \rho_0 \rightarrow A_\rho \cos(x/\xi - \theta_\rho) \exp(-x/\eta) \qquad (2)$$

Here ξ and η denote a characteristic wavelength and a correlation length, respectively, which are determined by the bulk structure of the fluid, while the amplitude A_ρ and phase θ_ρ depend on the particle-wall interaction. Following the model of Tarazona and Vicente,[28] the correlation length η, which governs the asymptotic decay, can be given in a particularly useful form as

$$\eta^{-1} = \sqrt{-S(q_0)/S''(q_0)} \quad (3)$$

Here $S(q)$ denotes the bulk structure factor, $S''(q)$ its second derivative, and q_0 the position of the first maximum of $S(q)$. Using eqn (3), the model of Fig. 3 gives $\eta \approx 5.4$ nm and $\eta \approx 4.7$ nm for reverse micelles #1 and #2, respectively. Hence, the amplitude of the density oscillations at a distance of one particle diameter is expected to decay rapidly, since $\exp(-\sigma/\eta) < 0.1$.

4 Concluding remarks

Finally, we comment on possible future applications of the grating-based holographic X-ray diffraction technique. The electron density contrast and particle size of the present study are close to those found in, for example, protein solutions. Moreover, the wettability of the confining surfaces can be modified. Hence, we foresee model-independent density profile reconstructions of various biologically relevant fluids confined between either hydrophobic or hydrophilic surfaces.

Acknowledgements

The experiment was carried out at the cSAXS beamline of the Swiss Light Source, Paul Scherrer Institut, Switzerland. We thank L. Strübin for assistance with the contact angle measurements.

References

1 J. Mittal, T. M. Truskett, J. R. Errington and G. Hummer, *Phys. Rev. Lett.*, 2008, **100**, 145901.
2 I. K. Snook and D. Henderson, *J. Chem. Phys.*, 1978, **68**, 2134.
3 J. N. Israelachvili, *Intermolecular and Surface Forces*, Academic Press, London, 2nd edn, 1991.
4 E. Perret, K. Nygård, D. K. Satapathy, T. E. Balmer, O. Bunk, M. Heuberger and J. F. van der Veen, *Europhys. Lett.*, 2009, **88**, 36004.
5 J. Als-Nielsen and D. McMorrow, *Elements of Modern X-ray Physics*, John Wiley and Sons, New York, 2001.
6 S. Jähnert, D. Müter, J. Prass, G. A. Zickler, O. Paris and G. H. Findenegg, *J. Phys. Chem. C*, 2009, **113**, 15201.
7 D. Müter, T. Shin, B. Demé, P. Fratzl, O. Paris and G. H. Findenegg, *J. Phys. Chem. Lett.*, 2010, **1**, 1442.
8 A. Poynor, L. Hong, I. K. Robinson, S. Granick, Z. Zhang and P. A. Fenter, *Phys. Rev. Lett.*, 2006, **97**, 266101.
9 K. Kashimoto, J. Yoon, B. Hou, C.-H. Chen, B. Lin, M. Aratono, T. Takiue and M. L. Schlossman, *Phys. Rev. Lett.*, 2008, **101**, 076102.
10 K. Nygård, D. K. Satapathy, O. Bunk, A. Diaz, E. Perret, J. Buitenhuis, F. Pfeiffer, C. David and J. F. van der Veen, *Opt. Express*, 2008, **16**, 20522.
11 K. Nygård, D. K. Satapathy, O. Bunk, E. Perret, J. Buitenhuis, C. David and J. F. van der Veen, *J. Appl. Crystallogr.*, 2009, **42**, 1129.
12 B. Tamamushi and N. Watanabe, *Colloid Polym. Sci.*, 1980, **258**, 174.
13 K. Nygård, O. Bunk, E. Perret, C. David and J. F. van der Veen, *J. Appl. Crystallogr.*, 2010, **43**, 350.
14 H. Schift, S. Saxer, S. Park, C. Padeste, U. Pieles and J. Gobrecht, *Nanotechnology*, 2005, **16**, S171.
15 P. Kraft, A. Bergamaschi, C. Broennimann, R. Dinapoli, E. F. Eikenberry, B. Henrich, I. Johnson, A. Mozzanica, C. M. Schlepütz, P. R. Willmott and B. Schmitt, *J. Synchrotron Radiat.*, 2009, **16**, 368.
16 D. I. Svergun, P. V. Konarev, V. V. Volkov, M. H. J. Koch, W. F. C. Sager, J. Smeets and E. M. Blokhuis, *J. Chem. Phys.*, 2000, **113**, 1651.
17 J. S. Pedersen, *J. Appl. Crystallogr.*, 1994, **27**, 595.
18 R. J. Baxter, *J. Chem. Phys.*, 1968, **49**, 2770.
19 D. K. Satapathy, O. Bunk, K. Jefimovs, K. Nygård, H. Guo, A. Diaz, E. Perret, F. Pfeiffer, C. David, G. H. Wegdam and J. F. van der Veen, *Phys. Rev. Lett.*, 2008, **101**, 136103.
20 D. K. Satapathy, K. Nygård, O. Bunk, K. Jefimovs, E. Perret, A. Diaz, F. Pfeiffer, C. David and J. F. van der Veen, *Europhys. Lett.*, 2009, **87**, 34001.
21 J. L. Parker, P. Richetti, P. Kékicheff and S. Sarman, *Phys. Rev. Lett.*, 1992, **68**, 1955.
22 B. Smit, P. A. J. Hilbers, K. Esselink, L. A. M. Rupert, N. M. van Os and A. G. Schlijper, *J. Phys. Chem.*, 1991, **95**, 6361.
23 B. Götzelmann, A. Haase and S. Dietrich, *Phys. Rev. E: Stat. Phys., Plasmas, Fluids, Relat. Interdiscip. Top.*, 1996, **53**, 3456.
24 M. C. Gerstenberg, J. S. Pedersen and G. S. Smith, *Phys. Rev. E: Stat. Phys., Plasmas, Fluids, Relat. Interdiscip. Top.*, 1998, **58**, 8028.
25 S. Karanikas, J. Dzubiella, A. Moncho-Jordá and A. A. Louis, *J. Chem. Phys.*, 2008, **128**, 204704.
26 R. Evans, R. J. F. Leote de Carvalho, J. R. Henderson and D. C. Hoyle, *J. Chem. Phys.*, 1994, **100**, 591.
27 S. H. L. Klapp, Y. Zeng, D. Qu and R. von Klitzing, *Phys. Rev. Lett.*, 2008, **100**, 118303.
28 P. Tarazona and L. Vicente, *Mol. Phys.*, 1985, **56**, 557.